Int. J. Electrochem. Sci., 12 **(2017)** 144 – 154, doi: 10.20964/2017.01.10

International Journal of
ELECTROCHEMICAL
SCIENCE
www.electrochemsci.org

Graphene-Enabled Improved Supercapacitor Performance of Polyaniline Nanofiber Composites

Ran Li[1], *Xiaoli Dong*[1], *Chengen He*[1], *Zixiu Liu*[1], *Leping Huang*[2,*], *and Yingkui Yang*[1,*]

[1] School of Materials Science and Engineering, Hubei University, Wuhan 430062, China
[2] School of Materials Science and Engineering, Wuhan Textile University, Wuhan 430200, China
[*]E-mail: lphuang@wtu.edu.cn, ykyang@hubu.edu.cn

Received: 29 September 2016 / *Accepted:* 13 November 2016 / *Published:* 12 December 2016

Graphene/PANI nanofiber composites were synthesized by *in-situ* chemical oxidative polymerization of aniline in the presence of graphene oxide (GO) followed by chemical reduction of GO. The as-synthesized composite was carefully characterized by the combination of the microscopy and spectroscopy techniques. The supercapacitor performance of graphene/PANI nanofiber composite was further investigated. As expected, the synergistic interactions between graphene and PANI enable the as-fabricated electrode with greatly improved electrochemical performance. The specific capacitance of graphene/PANI was calculated to be 952 F/g at 1 A/g, much higher than those of graphene (236 F/g) and PANI (621 F/g) counterparts. The specific capacitance maintains 645 F/g at 10 A/g with 68% retention of original capacitance after a 10-fold increase in the current density. Moreover, the graphene/PANI electrode remains 88% retention of initial capacitance over 1000 cycles, while PANI only gives 73% of original capacitance. These data clearly suggest that large capacitance, high rate capability, and good cycling stability can be synchronously achieved by doping PANI nanofibers with graphene sheets.

Keywords: Graphene, polyaniline, nanocomposites, supercapacitors

1. INTRODUCTION

Supercapacitors, as the next generation of energy-storage and power supply devices, have been developed to meet the increasing demand for applications in powering vehicles and portable electronic devices due to their high power density and long cycle-life.[1] There have been two classes of electrochemical capacitors based on the charge-storage mechanism, *i.e.*, electrical double-layer capacitors (EDLCs) and pseudo-capacitors, depending on the electrode materials used.[2] Among various materials used for supercapacitor electrodes, conducting polymers, typically including

polyaniline (PANI), polypyrrole, and polythiophene, have stimulated increasing interest owing to their large theoretical capacitances and high energy density.[3] Especially PANI has been considered as one of the most promising electrode materials for energy storage due to its easy of synthesis and low production cost.[4] PANI also presents a variety of morphological structures, such as one-dimensional nanofibers,[5-7] hollow microspheres,[8, 9] and hollow microtubes,[10, 11] which are usually dependent on the use of the oxidants and doping agents.[12] For instance, Zhang and co-workers [13] synthesized PANI nanofibers by an innovative free-template method using ferric chloride ($FeCl_3$) as the oxidant during chemical polymerization. However, such pseudo-capacitive materials often suffer from low power density due to low electrical conductivity and slow electron transfer kinetics, and low cycling stability and short lifetimes because of large volume change during doping/de-doping process.[14, 15] These factors have limited practical applications of supercapacitors based on conducting polymer electrodes.

The integration of carbonaceous nanomaterials with PANI has been successfully demonstrated to improve the electrochemical performance. Among carbon allotropes, graphene has attracted more attention over the past years due to its ultra-large specific surface area, high electronic conductivity, excellent chemical stability and electrochemical activity, and especially high theoretical specific capacitance (550 F/g).[16-18] Graphene also exhibits excellent compatibility with dissimilar materials such as metal oxides and conducting polymers, thereby enabling the fabrication of high-performance graphene-based composites *via* in-situ hybridization and *ex-situ* recombination.[19] In this work, graphene/PANI nanofiber composites were synthesized by *in-situ* chemical oxidative polymerization of aniline in the presence of graphene oxide (GO) followed by chemical reduction of GO. The resulted composite was further used as the supercapacitor electrode, and its electrochemical performance was investigated carefully. Herein graphene serves as a conducting pathway for rapid transportation of ionic species and electric charges throughout the composite electrode. The PANI nanofibers also prevent the agglomeration and stacking of graphene sheets, thereby affording large accessible surface and high electrochemical utilization of the electrode.[20] Moreover, flexbile graphene sheets can maintain the mechanical stability of the overall electrode during cycling process. Such synergistic effects enable the composite electrode with larger specific capacitance, higher rate capability, and better cyclability compared to the reduced GO (RGO) and PANI.

2. EXPERIMENTAL SECTION

2.1. Materials

Graphite power was purchased from Sigma Aldrich. Potassium persulfate ($K_2S_2O_8$), phosphorus pentoxide (P_2O_5), sodium nitrate ($NaNO_3$), potassium permanganate ($KMnO_4$), hydrochloric acid (HCl), hydrazine hydrate ($N_2H_4 \cdot H_2O$, 98%), hydrogen peroxide (H_2O_2), aniline, chloroform, and $FeCl_3$ were purchased from Sinopharm Chemical Reagent Ltd. Co. Sulfuric acid (H_2SO_4) was purchased from Tianjin Fuyu Chemical Ltd. Co. All chemicals were used without further purification.

2.2. Synthesis of graphene oxide (GO)

Graphite powder (6.0 g) was put into a mixture containing concentrated H_2SO_4 (50 mL), $K_2S_2O_8$ (5.0 g), and P_2O_5 (5.0 g). The solution was heated to 80°C and kept stirring for 4.5 h. The mixture was then diluted with deionized water (1 L) and cooled to room temperature. The pre-oxidized product was obtained by filtration using the 0.2 μm Nylon membrane followed by drying. The pre-oxidized graphite was treated by the Hummers method.[21, 22] The resulting graphite oxide jelly was then diluted to a suitable concentration and finally exfoliated into a homogeneous yellow-brown GO suspension under bath sonication for further use.

2.3. Preparation of RGO/PANI composites

A certain amount of aniline solution in chloroform was dispersed into the GO solution by ultra-sonication for 30 min before standing within 0-2°C ice bath. An aqueous solution of $FeCl_3$ (aniline: $FeCl_3$ = 6:1 in mole) was then added into the above suspension of GO and aniline with a speed of 3 drops/min. The resulted mixture was stirred for another 12 h in an ice bath. The product was collected by filtering and washing with deionized water until the filtrate becomes colourless. Furthermore, the resulting solid was dispersed into 100 mL deionized water under sonication for 30 min, and 200 μL of $N_2H_4 \cdot H_2O$ was slowly added into the suspension. After further reaction at 98°C for 1 h, the final RGO/PANI composite powder was achieved by filtration and washing with deionized water followed by vacuum-drying at 60°C. The proportion of GO to aniline is 1/2 in mass ratio in the reaction system. For comparison, pure RGO and PANI were also prepared with comparable methods.

2.4. Characterization

Transmission electron microscope (TEM) measurement was conducted on a Tecnai G220 electron microscope at 200 kV. Scanning electron microscope (SEM) measurement was carried out a scanning electron microanalyser (JSM6510LV) at 15.0 kV. Fourier transform infrared (FT-IR) spectra were performed on a Perkin-Elmer Spectrum One with KBr pellets. Raman spectra were performed over 500-4000 cm^{-1} with an excitation wavelength of 642.8 nm using RFS-100/S Raman spectrometer equipment. X-ray diffraction (XRD) experiments were conducted in a D/MAX-IIIC X-ray diffractometer with Cu Kα radiation.

All electrochemical performance measurements were carried out based on a conventional three-electrode system using a CHI760E electrochemical workstation at room temperature. Besides the saturated calomel reference electrode and platinum counter electrode, a modified glassy carbon electrode (3 mm in diameter dropped with 5 μL of 1 mg/mL composite suspension) was used as the working electrode, and 1 M H_2SO_4 aqueous solution as the electrolyte. The potential window ranges from -0.2 to 0.9 V for cyclic voltammetry (CV), and 0 to 0.8 V for Galvanostatic charge-discharge (GCD). The swept frequency of the EIS tests are from 100 KHz to 0.01 Hz with the applied amplitude is 5 mV versus the open circuit potential. The measurement of cycling stability was performed by cycling GCD at a current density of 1 A/g for 1000 cycling times.

3. RESULTS AND DISCUSSION

3.1. Synthesis and characterization of RGO/PANI nanofiber composites

Figure 1 shows typical TEM images of GO and RGO, and SEM images of PANI and RGO/PANI composites. RGO sheets (Fig. 1b) appear as a multilayer structure compared to the monolayer or few-layer of GO (Fig. 1a) due to the reduction-induced re-stacking in the presence of PANI. Pure PANI (Fig. 1c) shows typical nanofibers with 20-30 nm in diameter, comparable with the reported references.[6, 7, 13, 23] For RGO/PANI composites (Fig. 1d), PANI nanofibers are uniformly anchored on the RGO surface due to the π-π stacking, hydrogen bonding and electrostatic interactions between them. Graphene sheets not only provide a highly conductive network in the composite and also serve as a support for nanosized PANI fibers. Such an unique 3D architecture can reduce the diffusion path of ions transferring into the interior of PANI nanofibers to improve the electrochemical properties of the electrode materials.[18]

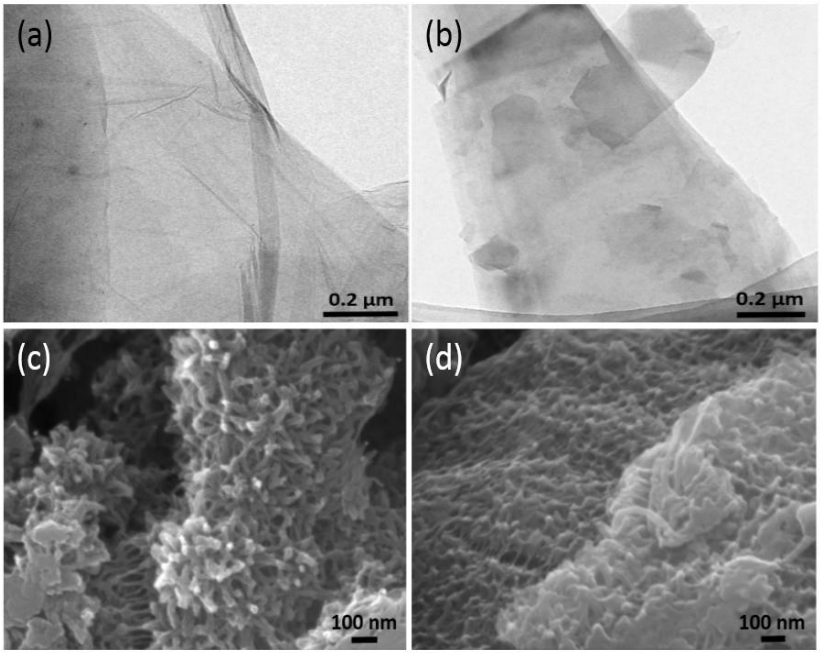

Figure 1. TEM images of GO (a) and RGO (b), and SEM images of pure PANI (c) and RGO/PANI (d).

Figure 2 shows the FT-IR spectra of GO, RGO, PANI and RGO/PANI. The Figure 2a for GO shows an obvious broad peak around 3354 cm^{-1} assigned to the O-H stretching vibration. This is related to the absorbed water by large amount of hydrophilic group in GO. Three peaks at 1729, and 1223 cm^{-1} correspond to the C=O, and C-O stretching vibrations, respectively.[9, 24] The peak of C=O in RGO almost disappears, and the vibration bands in the range of 1000-1200 cm^{-1} become weaker due to the reduction of GO as result of the less oxygen-containing groups.[25] For pure PANI, the peaks located at 1573, 1488, 1295, 1139, and 788 cm^{-1} correspond to the N–H and C=C stretching, the C-H in-plane deformation, the C-N stretching, and the C-H out-of-plane bending, respectively.[13] All of

these characteristic bands of PANI are clearly observed in RGO/PANI, indicating the existence of PANI in the composite.[26]

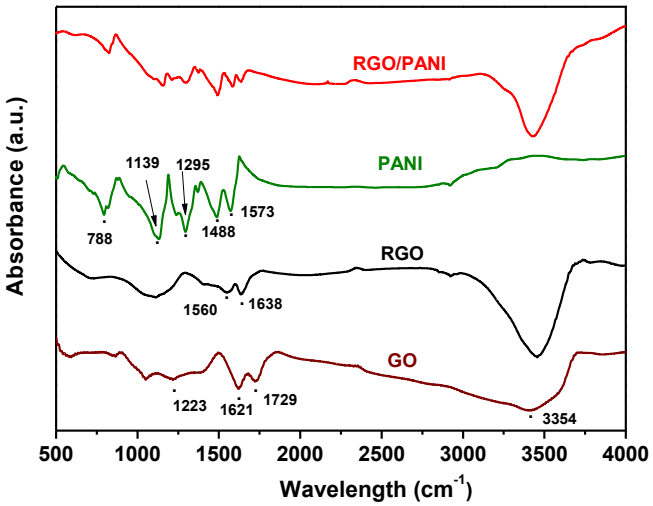

Figure 2. FT-IR spectra of GO, RGO, PANI, and RGO/PANI.

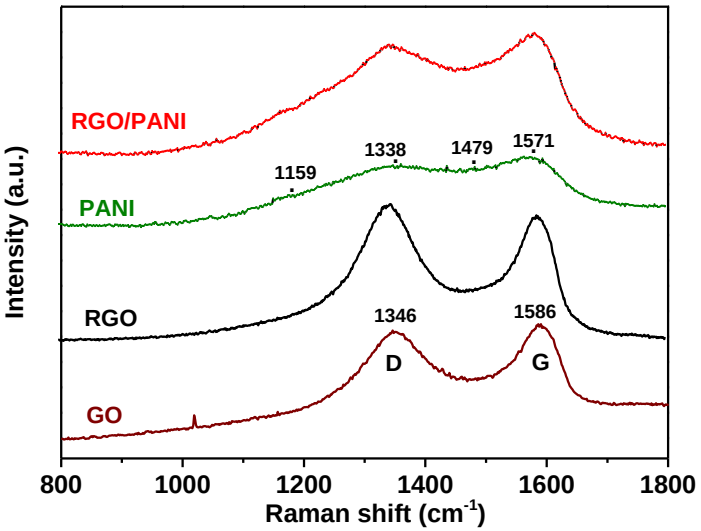

Figure 3. Raman spectra of GO, RGO, PANI, and RGO/PANI.

Figure 3 shows the Raman spectra of GO, RGO, PANI and RGO/PANI. GO and RGO show two prominent peaks at about 1350 and 1590 cm^{-1} corresponding to the D mode (for the sp^3-hybridized carbon) and G mode (for the sp^2-hybridized carbon), respectively.[27] The intensity ratio of D to G mode (I_D/I_G) in RGO is 1.07, which is a little higher than that of GO (0.95). This implies a decrease in the average size of sp^2 aromatic domains from graphene through the creation of numerous new graphitic domains during the reduction of GO.[27, 28] For pure PANI, the C-H vibration of quinoid ring, double polaron C-$N^{\cdot+}$ stretching, N-H bending, and C=C stretching vibrations of benzene were

observed at 1159, 1138, 1479 and 1571 cm^{-1}, respectively.[15, 29] The Raman bands for the RGO/PANI composite become clearly broad due to the overlapping of both D and G peaks of graphene with characteristic peaks of PANI.

Figure 4 shows the XRD patterns of GO, RGO, PANI and RGO/PANI. XRD patterns of GO exhibits a sharp peak at 2θ=11.0° with a corresponding interlayer spacing of 0.80 nm, which can be assigned to the (001) reflection peak.[30] For RGO, one broad peak centered at 2θ=24.7° corresponds to the interlayer spacing of 0.36 nm due to the removal of oxygen-containing groups from the surface of GO.[9, 14] For pure PANI, several broad reflection peaks at 2θ=14.9°, 20.2°, and 25.1°, correspond to its (011), (020), and (011) planes, respectively. This is consistent with the emeraldine salt crystallization of PANI nanofibers.[13] Characteristic peaks of PANI can be distinguished indistinctly in the RGO/PANI composite. The (002) peak of RGO shifts to 2θ=19.6° due to the fact that PANI coated on RGO expands the interlayer spacing,[3] in good accordance with the SEM results.

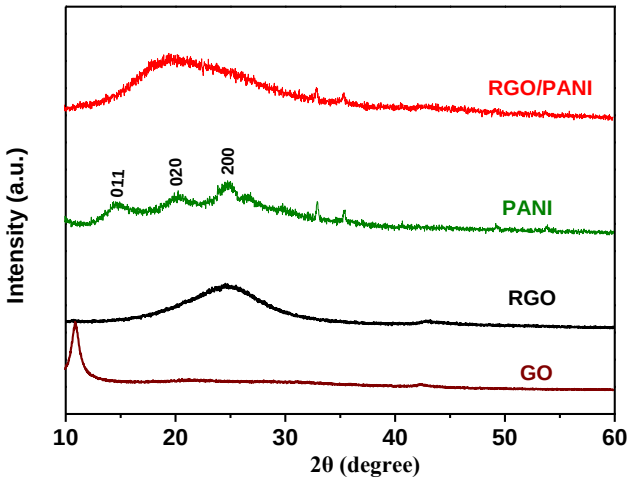

Figure 4. XRD patterns of GO, RGO, PANI, and RGO/PANI.

3.2. Electrochemical performance of RGO/PANI composite electrodes

Figure 5a shows the CV curves of PANI, RGO, and RGO/PANI electrodes at a scan rate of 10 mV/s in 1 M H_2SO_4. The CV cycle of RGO have no obvious redox peaks due to strong EDLC characteristics. In contrast, pure PANI and RGO/PANI have three pairs of redox peaks. The first oxidation peak C1 at -0.1~0.2 V during the positive-going potential scan is related to the well-known transition of PANI from the semiconducting-state (leucoemeraldine) to the conductive form (emeraldine). The C2 peak at 0.3~0.5 V corresponds to the overoxidation and hydrolysis of PANI to quinone-type species. The current from 0.6~0.8 V for the C3 peak is assigned to the second redox transition of PANI from the emeraldine to pernigraniline. Three corresponding peaks can be clearly observed during the reverse scan.[31-33] Of note, the integrated area and hence specific capacitance of RGO/PANI is much larger than those of pure PANI and RGO due to the enlarged specific surface area.

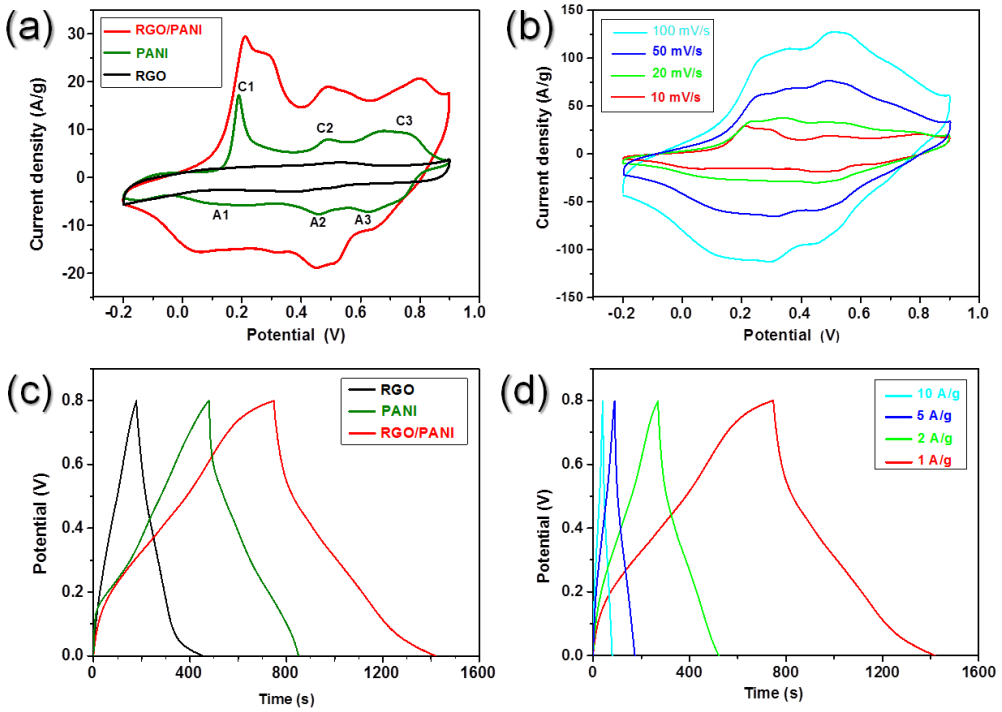

Figure 5. (a) CV curves of RGO, PANI, and RGO/PANI at a scan rate of 10 mV/s, (b) CV curves of RGO/PANI at scan rates of 10-100 mV/s, (c) GCD curves of RGO, PANI, and RGO/PANI at a current density of 1 A/g, and (d) GCD curves of RGO/PANI at current densities of 1-10 A/g.

Figure 5b further shows the CV curves of RGO/PANI at different scan rates. The response currents grow with increasing the scan rate from 10, 20, and 50 to 100 mV/s. The oxidation peaks gradually shift to the positive potential while the reduction peaks move to the negative potential due to the inadequate time for the ion migration at high scan rate. The specific capacitance based on the CV curve can be calculated by the following equation:

$$C_s = \frac{1}{vm(Va - Vc)} \int_{Va}^{Vc} I dV$$

where v is the scan rate (V/s), m is the active mass of electrode (g), and V_a-V_c is the voltage window (V). The specific capacitances were calculated to be 1226, 954, 781, and 663 F/g at 10, 20, 50, and 100 mV/s, respectively. These values are comparable and/or superior to the previously reported results.[34]

Figure 5c shows the GCD curves of PANI, RGO, and RGO/PANI samples with a potential window of 0-0.8 V at a current density of 1 A/g. The specific capacitances based on the GCD curves can be calculated by the following formula:

$$C_s = I \cdot \Delta t / (\Delta V \cdot m)$$

where I is the discharge current (A), Δt is the discharge time (s), ΔV is the voltage window (V), and m is the active mass of electrode (g). The specific capacitance of RGO, PANI, and RGO/PANI are 236, 621, and 952 F/g at 1 A/g, respectively. PANI has a higher specific capacitance compared to RGO due to its unique fibrous-network structure and inherent pseudocapacitive characteristics. Specific capacitance of RGO/PANI is much higher than the sum of RGO and PANI. Herein RGO plays an

important role as a backbone to build a 3D conductive network with an increased specific surface area and the effective utilization of PANI, thus enhancing the specific capacitance of the composite.

Figure 5d further gives the GCD curves of RGO/PANI at different current densities. Specific capacitances of RGO/PANI are 844, 715 and 645 F/g at 2, 5, and 10 A/g, respectively, and decrease with increasing the current density. The retention is up to 68%. The performance of RGO/PANI electrode is much better than those of graphene/PANI composites reported previously (see Table 1). RGO sheets provide a conductive network for electron transporting through the overall electrode while PANI nanofibers create an interconnected channel for electrolyte ions transfer in the active materials.

Table 1. Electrochemical performance of graphene/PANI composite electrodes

Composites	Capacitance (F/g)	Rate capability	Electrolyte	Ref.
PANI nanofiber/graphene	480 (0.1 A/g)	48.78% (1 A/g)	2M H_2SO_4	[34]
PANI/graphene paper	763 (1 A/g)	64.2% (10 A/g)	1M H_2SO_4	[35]
PANI nanofiber/graphene	610 (1 A/g)	57.4% (20 A/g)	1M H_2SO_4	[36]
PANI nanowire/GO	555 (0.2 A/g)	40.90% (2 A/g)	1M H_2SO_4	[37]
Mesoporous PANI/graphene	749 (0.5 A/g)	73% (5 A/g)	1M H_2SO_4	[38]
Hollow PANI/graphene	682.75 (0.5 A/g)	46.77% (10 A/g)	1M H_2SO_4	[39]
PANI nanorod/graphene	863.2 (0.2 A/g)	67.4% (5 A/g)	1M H_2SO_4	[40]
PANI nanofiber/graphene	952 (1 A/g)	68% (10 A/g)	1M H_2SO_4	This work

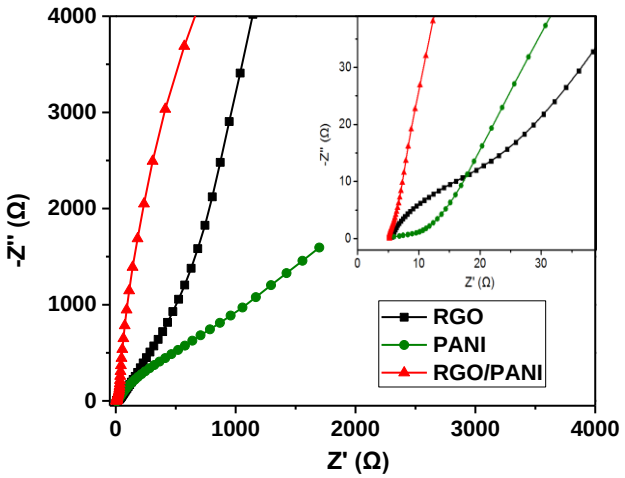

Figure 6. Nyquist plots of RGO, PANI, and RGO/PANI composite electrodes.

Figure 6 shows the EIS curves of pure PANI, RGO, and RGO/PANI composite electrodes measured with the swept frequency from 100 KHz to 0.01 Hz. All impedance spectra were composed of a semicircle at high frequencies and a straight line at low frequencies, indicating a typical capacitive behaviour.[3, 27] The intersection vale with the transverse at high frequency due to the solution resistance is about 4.7 Ω for all samples. The reaction resistance of RGO/PANI read from the diameter of the semicircle is remarkably small due to fast interface charge-transfer and redox-reactions.[29, 32]

At low frequency region, the line of RGO/PANI is nearly perpendicular to the lateral axis, suggesting a low resistance of ions diffusion because of high electronic conduction and ion migration in the 3D network created by RGO.[3, 27, 29]

Figure 7 shows the capacitance variation of RGO, PANI and RGO/PANI electrodes at 1.0 A/g for 1000 charge-discharge cycles. PANI maintains 73% of original capacitance because PANI is easy of electrochemical degradation during the charge-discharge process. In contrast, specific capacitance of RGO/PANI remains as high as 88% of initial capacitance after 1000 cycles, which is higher than 82% retention after 1000 cycles for graphene/PANI paper.[35] The excellent cycling stability can be explained as follows. The intimate combination between RGO sheets and PANI nanofibers can accelerate the charge transfer inside the composite electrode. RGO sheets also function as the frameworks and separators for supporting PANI nanofibers and accommodating the volume variation of swelling and shrinking during cycling, thereby achieving a significant improvement on the stability.

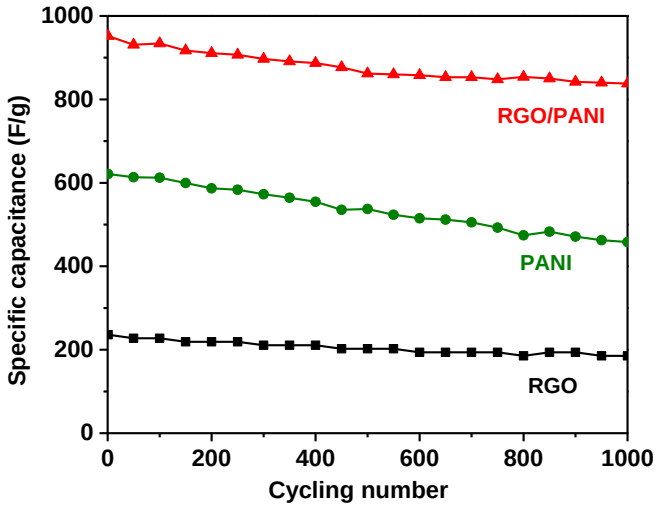

Figure 7. Cycle performance of RGO, PANI and RGO/PANI electrodes measured at 1 A/g for 1000 charge-discharge cycles.

4. CONCLUSIONS

Graphene/PANI nanofiber composite was successfully prepared by in-situ oxidative polymerization of aniline monomer in the presence of GO followed by chemical reduction of GO using hydrazine. The morphology, composition, and electronic structure of the composites together with PANI, GO, and RGO were characterized using TEM, SEM, Raman, FT-IR, and XRD techniques. In the composite, PANI nanofibers were uniformly anchored on the RGO surface. It was found that such composite is able to deliver large specific capacitance, high rate performance, and good cycling stability during charging-discharging process when used as the supercapacitor electrode. The specific capacitance for RGO/PANI is as high as 952 F/g at 1 A/g and remains 68% of capacitance at 10 A/g. The composite electrode can also maintain its specific capacitance up to 88% over 1000 cycles at 1

A/g. The as-prepared RGO/PANI composite therefore has promising application in high-performance supercapacitors.

ACKNOWLEDGMENTS
We thank the financial support from the National Natural Science Foundation of China (51273057), the Program for New Century Excellent Talents in University (NCET-12-0709), the Funds for Distinguished Young Scientists in Hubei (2015CFA048), and the Chutian Scholar Program of Hubei Province (China).

References

1. Z. Wang, X. He, S. Ye, Y. Tong, G. Li, *ACS Appl. Mater. Interfaces,* 6 (2014) 642.
2. H. Wang, Q. Hao, X. Yang, L. Lu, X. Wang, *ACS Appl. Mater. Interfaces,* 2 (2010) 821.
3. K. Zhang, L. Zhang, X. Zhao, J. Wu, *Chem. Mater.,* 22 (2010) 1392.
4. J. Yan, T. Wei, Z. Fan, W. Qian, M. Zhang, X. Shen, F. Wei, *J. Power Sources,* 195 (2010) 3041.
5. J. Huang, S. Virji, B. Weiller, R. Kaner, *J. Am. Chem. Soc.,* 125 (2003) 314.
6. N. Chiou, A. Epstein, *Adv. Mater.,*17 (2005) 1679.
7. J. Huang, R. Kaner, *J. Am. Chem. Soc.,* 126 (2004) 851.
8. B Mu, W Zhang, A Wang, *J. Nanopart. Res.,* 16 (2014) 2432.
9. N. Trung, T. Tam, H. Kim, S. Hur, E. Kim, W. Choi, *Chem. Eng. J.,* 255 (2014) 89.
10. H. Dong, S. Prasad, V. Nyame, W. Jones, *Chem. Mater.,* 16 (2004) 371.
11. N. Chiou, L. Lee, J. Epstein, *Chem. Mater.,* 19 (2007) 1589.
12. P. Yu, Y. Li, X. Zhao, L. Wu, Q. Zhang, *Langmuir,* 30 (2014) 5306.
13. Z. Zhang, M. Wan, Y. Wei, *Adv. Funct. Mater.,* 16 (2006) 1100.
14. Z. Gao, W. Yang, J. Wang, B. Wang, Z. Li, Q. Liu, M. Zhang, L Liu, *Energy Fuels,* 27 (2013) 568.
15. Z. Tong, Y. Yang, J. Wang, J. Zhao, B. Su, Y. Li, *J. Mater. Chem. A,* 2 (2014) 4642.
16. M. Carbone, L. Gorton, R. Antiochia, *Electroanalysis,* 27 (2015) 16.
17. F. Yan, M. Zhang, J. Li, *Adv. Healthcare Mater.,* 3 (2014) 313.
18. X. Dong, J. Wang, J. Wang, M. Park, X. Li, L. Wang, W. Huang, P. Chen, *Mater. Chem. Phys.,* 134 (2012) 576.
19. Y. Yang, C. Han, B. Jiang, J. Iocozzia, C. He, D. Shi, T. Jiang, Z. Lin, *Mater. Sci. Eng. R,* 102 (2016) 1.
20. T. Lee, T. Yun, B. Park, B. Sharma, H. Song, B. Kim, *J. Mater. Chem.,* 22 (2012) 21092.
21. W. Hummers, R. Offeman, *J. Am. Chem. Soc.,* 80 (1958) 1339.
22. N. Kumar, H. Choi, Y. Shin, D. Chang, L. Dai and J. Baek, *ACS Nano,* 6 (2012) 1715.
23. X. Zhang, W. Goux, S. Manohar, *J. Am. Chem. Soc.,* 126 (2004) 4502.
24. Y. Xu, H. Bai, G. Lu, C. Li, G. Shi, *J. Am. Chem. Soc.,* 130 (2008) 5856.
25. H. Wang, Q. Hao, X. Yang, L. Lu, X. Wang, *Electrochem. Commun.,* 11 (2009) 1158.
26. A. MacDiarmid, G. Chiang, A. Richter, *Synth. Met.,* 18 (1987) 285.
27. Y. Liu, Y. Ma, S. Guang, H. Xu, X. Su, *J. Mater. Chem. A,* 2 (2014) 813.
28. C. He, S. Sun, H. Peng, C. Tsui, D. Shi, X. Xie, Y. Yang, *Composites Part B,* 106 (2016) 81.
29. X. Liu, P. Shang, Y. Zhang, X. Wang, Z. Fan, B. Wang, Y. Zheng, *J. Mater. Chem. A,* 2 (2014) 15273.
30. Z. Liu, Z. Wang, X. Yang, *Langmuir,* 18 (2002) 4926.
31. F. Montilla, M. Cotarelo, E. Morallón, *J. Mater. Chem.,* 19 (2009) 305.

32. L. Pan, G. Yu, D. Zhai, H. Lee, W. Zhao, N. Niu, H. Wang, B. Tee, Y. Shi, Y. Cui, Z. Bao, *Proc. Natl. Acad. Sci.,* 109 (2012) 9287.
33. Y. Wang, H. Li, Y. Xia, *Adv. Mater.,* 18 (2006) 2619.
34. D. Wang, F. Li, J. Zhao, W. Ren, Z. Chen, J. Tan, Z. Wu, I. Gentle, G. Li, H. Cheng, *ACS Nano,* 3 (2009) 1745.
35. K. Zhang, L. Zhang, X. Zhao, J. Wu, *Chem. Mater.*, 22 (2010) 1392.
36. J. Luo, W. Zhong, Y. Zou, C. Xiong, W. Yang, *J. Power Sources,* 319 (2016) 73.
37. J. Xu, K. Wang, S. Zu, B. Han, Z. Wei, *ACS Nano*, 4 (2010) 5019.
38. Q. Wang, J. Yan, Z. Fan, T. Wei, M. Zhang, X. Jing, *J. Power Sources*, 247 (2014) 197
39. X. Liu, N. Wen, X. Wang, Y. Zheng, *ACS Sustainable Chem. Eng.*, 3 (2015) 475.
40. X. Liu, Y. Zheng, X.Wang, *Chem. Eur. J.*, 21 (2015) 10408.
41. H. Cong, X. Ren, P. Wang, S. Yu, *Energy Environ. Sci.*, 6 (2013) 1185.